

# Cd in SnO: Probing structural effects on the electronic structure of doped oxide semiconductors through the electric field gradient at the Cd nucleus

Leonardo A. Errico\* and Mario Rentería†

Departamento de Física-Instituto de Física La Plata (CONICET), Facultad de Ciencias Exactas, Universidad Nacional de La Plata, Casilla de Correo No. 67, 1900 La Plata, Argentina

Helena M. Petrilli‡

Instituto de Física-DFMT, Universidade de São Paulo, Caixa Postal 66318, São Paulo, 05315-970 São Paulo, Brazil

(Received 22 December 2006; revised manuscript received 17 February 2007; published 27 April 2007)

We perform an *ab initio* study of the electric field gradient (EFG) at the nucleus of Cd impurities at substitutional Sn sites in crystalline SnO. The full-potential linearized-augmented plane wave and the projector augmented wave methods used here allow us to treat the electronic structure of the doped system and the atomic relaxations introduced by the impurities in the host in a fully self-consistent way using a supercell approach in a state-of-the-art way. Effects of the impurity charge state on the electronic and structural properties are also discussed. Since the EFG is a very subtle quantity, its determination is very useful to probe ground-state properties such as the charge density. We show that the EFG is very sensitive to structural relaxations induced by the impurity. Our theoretical predictions are compared with available experimental results.

DOI: [10.1103/PhysRevB.75.155209](https://doi.org/10.1103/PhysRevB.75.155209)

PACS number(s): 71.15.-m, 76.80.+y, 71.20.-b, 71.55.Ht

## I. INTRODUCTION

The study of SnO and SnO<sub>2</sub> has been a topic of interest in the last few years due to their considerable technological importance and industrial applications. In fact, tin dioxide is used in many devices where transparent semiconductors are needed, such as thin heat reflecting foils, transparent electrodes, gas sensors, and solar panels, among others. Applications of SnO have been less frequent due to its tendency to decompose into metallic Sn and SnO<sub>2</sub> at high temperatures. As a consequence, in the past, the physical properties of SnO have not been studied in detail as in the case of SnO<sub>2</sub>. However, in the very last few years, several experimental and theoretical studies of tin monoxide were published in order to analyze its electronic structure and to discuss the differences between the two tin oxides.<sup>1-7</sup> In this sense, it was reported that epitaxial thin films of SnO grown by electron-beam deposition show *p*-type conduction, in contrast with the *n*-type behavior of SnO<sub>2</sub>.<sup>8</sup> Theoretical studies suggest that the *p*-type conductivity of tin monoxide originates from tin vacancies.<sup>2</sup> This is a very interesting result, since transparent oxides with *p*-type conductivity could produce different applications.<sup>9</sup> Both amorphous and crystalline tin oxide films are used in technological applications. Since optical, electric, and electronic properties are found to be dependent on the crystalline state of the films, it is important to study all stages in the amorphous-crystalline transition. Another interest is related to the fact that in most cases, impurities are included in order to improve the response of the material. In this sense, as an example, the interest in SnO<sub>2</sub> was recently renewed due to the discovery of high-temperature ferromagnetism in Sn<sub>1-x</sub>Co<sub>x</sub>O<sub>2-δ</sub> films,<sup>10</sup> with potential applications in spintronics. The impurities can introduce atomic relaxations in the host lattice and impurity levels in the gap of the semiconductor, modifying the electronic structure of the system. The description of these impurity levels (and their charge states) has attracted much interest.

One way to investigate structural, electronic, and magnetic properties at the atomic scale is by using hyperfine techniques.<sup>11</sup> Nuclear methods and, in particular, the time-differential perturbed-angular correlations (PAC) technique have been extensively applied to study materials to elucidate the (sub)nanoscopic scale environment(s) of impurities or constituent atoms of solids (see, e.g., Refs. 12–15). In the case of PAC, a suitable probe isotope (generally an impurity in the system under study) is used and the information provided, at this probe site, is given as a product of a nuclear and an extra nuclear quantity. In the case of electric quadrupole interactions, the nuclear quantity is the nuclear quadrupole moment ( $Q$ ), characteristic of a given nuclear state of spin  $I$ , which interacts with the electric field gradient (EFG) at the nuclear position. The information extracted from a PAC experiment is usually expressed as the nuclear quadrupole frequency  $\omega_Q$  and the asymmetry parameter  $\eta$ .<sup>11</sup>

Local and very accurate information about a system under study, provided by the EFG tensor, can be obtained by confronting experimental results with an accurate calculation of the EFG.<sup>16</sup> This is possible through the use of an all-electron (AE) *ab initio* electronic structure calculation in the framework of the density-functional theory (DFT).<sup>17</sup> Indeed, by performing a theoretical electronic structure calculation, we can obtain the EFG at a given site, which can be compared with experimental results. We can investigate, in this way, local properties such as location of defects and impurities and determine structural parameters, impurity energy levels, etc.<sup>13-16,18-22</sup> Since the EFG is very sensitive to the anisotropic charge distribution close to the probe nucleus, for its accurate calculation the entire electronic configuration of the host, perturbed by the presence of the impurity, has to be determined. In this research direction, some of us have studied Cd in different binary oxides, such as rutile TiO<sub>2</sub> (Refs. 13 and 14) and SnO<sub>2</sub> (Ref. 18), In<sub>2</sub>O<sub>3</sub> (Ref. 19), Lu<sub>2</sub>O<sub>3</sub> (Ref. 20), and Al<sub>2</sub>O<sub>3</sub> (Ref. 21).

In 1991, Rentería *et al.*<sup>23</sup> performed a series of PAC and Mössbauer spectroscopy experiments in Sn-O thin films that afterward underwent different oxidation thermal treatments in air. In those experiments, the authors found that in the thin films, two oxidation states of Sn coexist. Furthermore, the initially disordered SnO and SnO<sub>2</sub> phases were transformed into the crystalline and transparent SnO<sub>2</sub> phases by appropriate annealing treatments. The hyperfine parameters of <sup>111</sup>Cd in a crystalline SnO<sub>2</sub> thin film were obtained, confirming the results reported by Wolf *et al.*<sup>24</sup> in high-purity SnO<sub>2</sub> polycrystalline samples. However, the hyperfine interaction parameters of <sup>111</sup>Cd located at an undisturbed SnO environment could not definitely be characterized. In an ordered system with a known crystal structure, the interpretation of the experimental results is usually not too difficult. In the case of disordered or amorphous materials or multiphase samples (as the thin films studied in the SnO:Cd PAC experiments), multiple interactions may be observed and there are no straightforward interpretations and crude assumptions on the site assignments are made which can conduce to wrong conclusions. To unravel these complex cases, a realistic theory can be of great help since EFG calculations assuming different structural and electronic scenarios can be performed and compared with experimental results.

In this work, we report a DFT study of the EFG at Cd impurities located at the cation site in the semiconductor SnO using two state-of-the-art *ab initio* AE methods, the full-potential linearized-augmented plane wave<sup>25</sup> (FPLAPW) and the projector augmented wave (PAW) methods.<sup>26</sup> The predictions for the EFG tensor are compared with the available experimental PAC results.<sup>23</sup> Our calculations suggest that new experiments are necessary in order to characterize the EFG tensor at Cd impurities in SnO. We illustrate the importance of EFG calculations, not only for the description of the physical properties of the impurity-host system but also for the interaction assignments. The effects of the impurity charge state on the electronic and structural properties of this doped system are discussed.

This paper is organized as follows. In Sec. II, we describe the system under study and the methods of calculation. In Sec. III, we review and discuss experimental and theoretical results obtained in pure SnO, while in Sec. IV, we present our results for the structural and electronic properties of Cd-doped SnO. In Sec. V, we discuss the effects of the charge state of the impurity on these electronic and structural properties. Finally, in Sec. VI, we present our conclusions.

## II. THEORETICAL APPROACH

The EFG is a traceless symmetric tensor of rank 2 whose components, denoted by  $V_{ij}$ , are defined by the second derivative (with respect to the spatial coordinates) of the Coulomb potential  $V(\vec{r})$  created by the charge density surrounding a given nucleus,

$$V_{ij}(\vec{r}=0) = \left. \frac{\partial^2 V}{\partial^2 x_i \partial x_j} \right|_{\vec{r}=0}. \quad (1)$$

The EFG can be determined straightforwardly once the total charge distribution has been accurately calculated. The

conventional choice is  $|V_{XX}| \leq |V_{YY}| < |V_{ZZ}|$  in the principal-axis system. Hence,  $V_{ZZ}$  is the largest eigenvalue of the EFG tensor, and the asymmetry parameter  $\eta$  is defined by the remaining two eigenvalues  $V_{XX}$  and  $V_{YY}$ ,

$$\eta = \frac{V_{XX} - V_{YY}}{V_{ZZ}}. \quad (2)$$

$V_{ZZ}$  is related to the *nuclear quadrupole frequency*  $\omega_Q$  obtained in a PAC experiment through

$$\omega_Q = \frac{eQ}{4I(2I-1)\hbar} V_{ZZ}. \quad (3)$$

Here,  $Q$  is the nuclear quadrupole moment of the sensitive PAC state characterized by a nuclear-spin quantum number  $I$  (in this case, the  $I=5/2+151$  keV excited state of <sup>111</sup>Cd) and  $e$  is the proton's charge.

In the case of the Mössbauer experiment which we will discuss in the next section, due to the nuclear spin ( $I=3/2+$ ) of the sensitive state of <sup>119</sup>Sn, an independent experimental determination of  $V_{ZZ}$  and  $\eta$  is not possible. The measured magnitude is the *quadrupole splitting*  $\Delta_{eQ}$ , which is related to  $V_{ZZ}$  and  $\eta$  by

$$\Delta_{eQ} = \frac{eQ}{2} V_{ZZ} \left( 1 + \frac{\eta^2}{3} \right)^{1/2}, \quad (4)$$

where  $Q$  is the nuclear-quadrupole moment of the sensitive 24 keV excited state of <sup>119</sup>Sn.

Our aim here is to obtain from first-principles calculations the EFG at a Cd impurity replacing Sn in crystalline black SnO, properly taking into account the structural and electronic effects introduced by the impurity in the host lattice. We have simulated this nonperiodic system considering a periodically repeated large unit cell where a single Cd atom replaces a single Sn in the SnO host. We performed *ab initio* electronic structure calculations to determine the self-consistent potential and the charge density inside the cell.

SnO is tetragonal [ $a=b=3.799\ 82(9)$  Å,  $c=4.816(1)$  Å, and  $c/a=1.27$  (see Ref. 27)] in its most common variety (black SnO). The unit cell contains 2 f.u. with the oxygen atoms placed at (0;0;0) and (1/2;1/2;0) and tin atoms at (0;1/2;- $u$ ) and (1/2;0; $u$ ) with  $u=0.2374(8)$  (Ref. 27). In Fig. 1(a) we represent a portion of this oxide. The structure of SnO is made of layers and each Sn atom is at the apex of a square pyramid whose base is formed by four oxygen atoms [see Fig. 1(b)]. All Sn-nearest oxygen neighbor (Onn) distances are equal to 2.22 Å. Each oxygen ion is surrounded tetrahedrally by four Sn ions. The supercell (SC) considered in the present work consists of eight unit cells of SnO with one Sn atom replaced by the Cd impurity atom. The resulting 32-atom SC has dimensions  $a'=2a=b'=2b=7.599\ 64$  Å and  $c'=2c=9.632$  Å.

We used two different *ab initio* methods, FPLAPW (Ref. 25) and PAW,<sup>26</sup> to solve the Kohn-Sham equations in the framework of the DFT. In the first case, the electronic-structure calculations were performed with the WIEN97 code<sup>28</sup> in a scalar relativistic version without spin-orbit coupling. Exchange and correlation effects were treated within DFT using both the local-density approximation<sup>29</sup> (LDA)

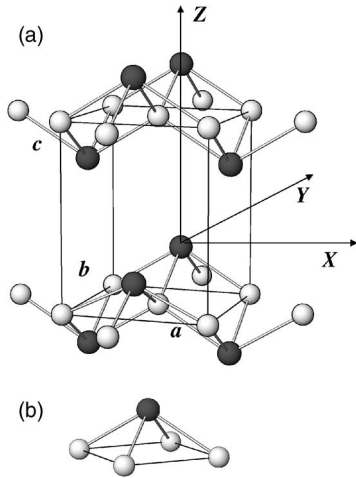


FIG. 1. (a) Simplified ball and stick model of the crystalline structure of SnO. (b) Nearest-neighbor oxygen (O<sub>nn</sub>) distribution around the cationic sites in SnO. In both cases, black balls represent Sn atoms and gray balls oxygen atoms.

and the generalized gradient approximation<sup>30</sup> (GGA). The atomic sphere radii used for Cd, Sn, and O were 1.06, 1.06, and 0.85 Å, respectively. We took for the parameter  $RK_{max} = R_{mt}K_{max}$ , which controls the size of the basis set in these calculations, the value of 7.0 ( $R_{mt}$  is the smallest muffin-tin radius and  $K_{max}$  the largest wave number of the basis set). We also introduced local orbitals to include Sn 4*d* and Sn 5*p*, O 2*s*, and Cd 4*p*, and Cd 4*d* orbitals. Integration in reciprocal space was performed using the tetrahedron method taking 60 *k* points in the first Brillouin zone ( $3 \times 3 \times 3$  *k*-point grid). Atomic displacements around the impurity have been obtained in the standard way described elsewhere.<sup>14</sup> The final forces on the ions were below the tolerance value of 0.01 eV/Å. At each position, the  $V_{ii}$  elements of the EFG tensor were obtained directly from the  $V_{2M}$  components of the lattice harmonic expansion of the self-consistent potential.<sup>31</sup>

To check the accuracy of our results, we have performed several additional calculations. For selected situations among the cases that we will describe in the next sections, we performed calculations varying the basis set from  $RK_{max} = 6.0$  to  $RK_{max} = 8.0$ , increased the number of *k* points to 250 ( $6 \times 6 \times 5$  *k*-point grid), and varied the muffin-tin radii. We observed that none of the factors considered influence qualitatively the results. Our tests show that, for  $RK_{max} = 7.0$  and 60 *k* points, the distances Cd-Onn are converged in less than 0.01 Å and the EFG components are converged within  $0.1 \times 10^{21}$  V/m<sup>2</sup>.

In addition to the FPLAPW calculations, we have used in our study the PAW method as embodied in the CP-PAW code developed by P. Blöchl *et al.*<sup>26</sup> The PAW method has been described elsewhere<sup>26,32,33</sup> and here we just summarize the main ingredients. PAW is an AE method that in the CP-PAW code is implemented in combination with the Car-Parrinello *ab initio* molecular-dynamics approach<sup>34</sup> with dampened motion to determine the electronic structure and atomic positions. The basis set is constituted by plane waves and localized functions, which preserves the information about the

characteristic wave-function nodal structure in the regions near the nuclei. PAW uses the idea of “augmentation” from the AE augmented wave methods<sup>26</sup> as FPLAPW does. The augmentation is specified by the so-called projector functions. Frozen core states were imported from the isolated atoms and the self-consistent calculations take into account a total charge density, which includes the core state density.<sup>26</sup> The EFG in PAW is obtained directly from the second derivative of the full potential, which is described in detail in Ref. 32. Besides the different basis functions used by the FPLAPW and PAW methods, one of the main differences among the WIEN97 and the CP-PAW codes used here is that the equilibrium atomic positions and electronic structure are obtained by the Carr-Parrinello approach<sup>34</sup> in the CP-PAW code, whereas in the WIEN97 code, after each self-consistent cycle, in which the diagonalization of the Hamiltonian is made, the forces are calculated and the atoms moved. The CP-PAW and WIEN97 results for the EFG have been shown to agree very well with each other and with experimental results in many different systems.<sup>32,35,36</sup>

The PAW calculations were performed using 3*s*, 3*p*, and 3*d* projectors for Sn and 2*s*, 2*p*, and 1*d* projectors for O. The suitability of these projectors for Sn and O atoms were carefully studied in Ref. 36. For Cd, we used 3*s*, 3*p*, and 3*d* projectors. The value of the plane waves cutoff energy (EPWPSI) was set as 60 Ry, and we used a grid of  $5 \times 5 \times 5$  *k* points. We performed a careful study of the convergence of EPWPSI and the *k*-point sampling. For EPWPSI=60 Ry and a grid of  $6 \times 6 \times 6$  *k* points the EFG tensor and the Cd-Onn distances are converged in less than  $0.1 \times 10^{21}$  V/m<sup>2</sup> and  $5 \times 10^{-3}$  Å, respectively.

Exchange and correlation effects were treated using both the LDA and the GGA.<sup>29,30</sup> We have chosen to present here only the results obtained with the PAW method using the GGA functional since the results obtained using the LDA functional follows, in general, the same trend.

### III. PRELIMINARY STUDY: UNDOPED SNO

The structural and electronic properties of pure black SnO were studied by different groups and also by some of us (see Refs. 1–8, 36, and 37), both theoretically and experimentally. Before proceeding with the study of the doped system, it is worth resuming, for easy reference, the main results we have obtained for the pure system.

Concerning the structural properties, the optimized *c/a* ratio and *u* predicted by our FPLAPW calculations are 1.24 (1.24) and 0.2366 (0.2361), when using the GGA (LDA) functional.<sup>37</sup> PAW calculations were also performed for this system without optimizing the lattice constants and we obtained *u*=0.2390.<sup>36</sup> Since all these results are in excellent agreement both with experiments<sup>27</sup> and previous calculations performed with the full-potential linear-muffin-tin-orbital (FPLMTO) method,<sup>4,6</sup> we have checked that both FPLAPW and PAW methods, in the present implementations, correctly describe the structural properties of SnO.

The density of states (DOS) of SnO obtained using the WIEN97 code is shown in Fig. 2(a). The DOS and the overall band structure obtained in our calculations are consistent

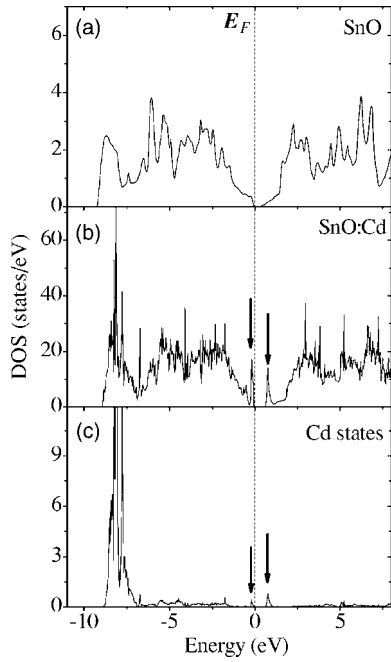


FIG. 2. Density of states for the unrelaxed structures in (a) pure SnO and [(b) and (c)] Cd-doped SnO. (c) is the projected density of states at the Cd site. Energies are referred to the Fermi level ( $E_F$ ), shown by a vertical dotted line. The arrows indicate impurity levels induced by Cd at the top of the valence band and at the bottom of the conduction band.

with theoretical results obtained using the FPLMTO (Ref. 6) method and the discrete variational method<sup>7</sup> (DVM). Both LDA and GGA functionals used in the FPLAPW calculations furnish an indirect band gap of about 0.3 eV, whereas the minimum direct gap is around 2.0 eV; the same is observed in the CP-PAW calculations (using GGA). As shown in Ref. 4, the band gap of SnO is very much pressure dependent and, in all theoretical calculations presented in the literature, the band gap of the equilibrium structure presents the same (small) order of magnitude. Although it is usually assumed that SnO is a semimetal or a small gap semiconductor, an optical gap in the order of 3.0 eV has been measured,<sup>38</sup> but a value of 0.7 eV has been mentioned in the literature.<sup>39</sup> The underestimation of the band gap, especially in metal oxides, is a well-known deficiency of LDA (and GGA), but this may not interfere with the calculation of observables that depend only on the ground state as, for example, the EFG. The valence band has mainly O  $2p$ , Sn  $5s$ , and Sn  $5p$  characters that evidence the covalent nature of the Sn-O bonds. The conduction band is predominantly Sn  $5p$ .

The  $V_{ZZ}$  component of the EFG tensor at the Sn site in undoped SnO we obtained using FPLAPW (Ref. 37) with the GGA (LDA) functional is  $-17.75 \times 10^{21}$  V/m<sup>2</sup> ( $-17.29 \times 10^{21}$  V/m<sup>2</sup>) and using the PAW method<sup>36</sup> (with GGA),  $V_{ZZ} = -17.2 \times 10^{21}$  V/m<sup>2</sup>. In all cases, the  $V_{ZZ}$  orientation is  $[0\ 0\ 1]$  and, in agreement with the symmetry of the considered site,  $\eta = 0.00$ . We note that in the CP-PAW code, no symmetry constraints are imposed. These results can be compared with other theoretical  $V_{ZZ}$  results available in the literature  $[-16.37, -17.6, \text{ and } -38.3 \times 10^{21}$  V/m<sup>2</sup> using, re-

spectively, the FPLMTO method,<sup>6</sup> FPLAPW method,<sup>40</sup> and DVM (Ref. 7)] and with the experimental result of  $20.0 \times 10^{21}$  V/m<sup>2</sup> obtained for the <sup>119</sup>Sn isotope through Mössbauer experiments.<sup>41</sup> The sign of the measured value 1.365 mm/s for  $\Delta_{eQ}$  is unknown, and the nuclear-quadrupole moment  $Q = -0.109(8)$  b (Ref. 42) of the sensitive 24 keV excited state of <sup>119</sup>Sn was used here to infer the experimental value of  $V_{ZZ}$  using Eq. (4) and assuming  $\eta = 0.00$ . The FPLAPW, PAW, and FPLMTO predictions for  $V_{ZZ}$  are in very good agreement with the experimental results. On the other hand, the cluster method calculation predicts a  $V_{ZZ}$  two times larger, so we see that the use of a full-potential approach is important to correctly reproduce the EFG in the metal oxides.

After these preliminary remarks, we have checked that the presently used FPLAPW and PAW implementations are able to correctly describe the EFG in pure SnO, giving us a solid basis to start the calculations for the Cd-doped system.

#### IV. CD-DOPED SNO

After the validation of the present approach through the study of the undoped SnO, we have replaced a Sn by a Cd atom in the SC, as described in Sec. II. As a first step, we have obtained the self-consistent electronic structure of this system with all atoms in their initial unrelaxed positions. The corresponding total DOS is shown in Fig. 2(b), and the projected DOS (PDOS) at the Cd site is shown in Fig. 2(c). Comparison of Figs. 2(a) and 2(b) shows that the presence of the Cd impurity induces the appearance of Cd  $4d$  levels and impurity states at the top of the valence band and at the bottom of the conduction band [indicated by arrows in Figs. 2(b) and 2(c)] in the corresponding DOS. We can also see that the state located at the top of the valence band (just below the Fermi level) is completely filled, while the impurity level at the bottom of the conduction band is empty, and the energy separation between them is around 0.65 eV. To analyze the orbital decomposition of the impurity states, we show in Fig. 3 the PDOS for Cd and its Onn. From this figure, we see that the characters of the two impurity states are slightly different. The state at the top of the valence band has Cd  $s$ , Cd  $p_z$ , and Onn  $p_x$ , Onn  $p_y$ , and Onn  $p_z$  characters. The second impurity level, located at the bottom of the conduction band, has Cd  $s$ , Cd  $p_z$ , Cd  $d_{z^2}$ , and Onn  $p_y$  and Onn  $p_z$  characters. In both cases, a small contribution from Sn  $s$  (not shown here) is also involved.

We calculated the EFG tensor at the unrelaxed positions. As can be seen from the results presented in Table I, the substitution of an indigenous Sn atom by a Cd impurity produces a significant change in the EFG tensor ( $V_{ZZ}$  varies from  $-17.3 \times 10^{21}$  V/m<sup>2</sup> at the Sn site to  $+7.7 \times 10^{21}$  V/m<sup>2</sup> at the Cd site). The symmetry and orientation of the EFG tensor are not changed. This huge difference in the EFG magnitude just illustrates the dominant electronic contribution to the EFG arising from the different electronic structures of Sn and Cd at this site. It is important to note that all calculations performed here predict the same EFG, so we can conclude (due to the fact that the EFG is very sensitive to small changes in the electronic charge density) that the

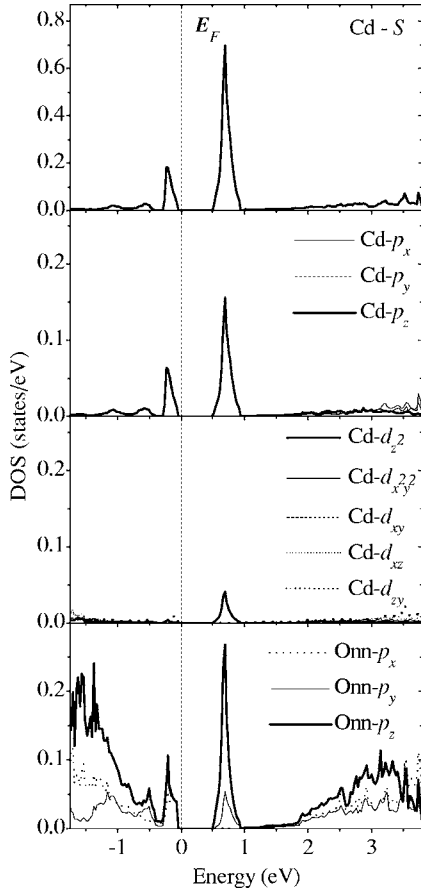


FIG. 3. Atom resolved PDOS for Cd and Onn in the unrelaxed 32-atom SC of SnO. Energies are referred to the Fermi level ( $E_F$ ).

descriptions of the electronic structure predicted by these calculations are very similar. In all EFGs at the Cd sites studied here (and in the next section), the so-called “valence”<sup>31</sup> EFG dominates, being almost negligible, the “semicore”  $s-d$  and higher  $l$  contributions as well as the “lattice” term. We found that the Cd  $p$  ( $5p$ ) contribution dominates over the  $d$  contri-

bution accordingly with the fact that the first node of the  $5p$  wave function is at much shorter distance than the one of the  $4d$  wave function<sup>31</sup> in this case.

The substitution of a Sn atom by a Cd impurity produces non-negligible forces on its nearest neighbors. In order to study the relaxation introduced by the impurity, we have considered the Cd and the Onn displacements until forces vanished using the WIEN97 code. We have performed two different relaxation process: (a) allowing the relaxation of the Onn atoms, keeping fixed the other atoms of the SC and (b) relaxing all atoms in the SC. We found that the amount of structural relaxation per atom decreases rapidly from the Onn to further shells, leading to minor changes in the positions of the Onn atoms. The EFG at the Cd site is essentially not affected by the relaxation of atoms lying beyond the Onn distance. Due to this fact none of the conclusions of the present study are affected by the displacement of atoms which lie beyond the Onn distance; thus we will not mention it in what follows.

As we can see from the results presented in Table I, the Onn relaxes outward, enlarging the basal plane in the directions  $a-b$  (see Fig. 1). The displacement of each of these Onn atoms obtained with the WIEN97 code and LDA is 0.05 Å (2.2% of the unrelaxed Cd-Onn distance). Additionally, we found that the impurity moved out from the symmetry site (0.02 Å), approaching the oxygen’s plane. The calculations performed with the WIEN97 code using the GGA approximation furnish a rather large relaxation of the Onn (0.09 Å). These structural distortions induced by the Cd impurity could be expected from a simple size effect analysis, since structural relaxations around impurities were also found in other Cd-doped binary oxides: for Cd at both cationic sites in  $\text{In}_2\text{O}_3$  (Ref. 19) and  $\text{Lu}_2\text{O}_3$  (Ref. 20), the impurity produced relaxations of around 0.1 Å; larger relaxations, in the range of 0.20–0.25 Å, were found in Cd-doped rutile  $\text{TiO}_2$  (Refs. 13 and 14), in  $\text{SnO}_2$  (Ref. 18), and in  $\text{Al}_2\text{O}_3$ .<sup>21</sup> All these relaxations can be explained noting that the bond length of the sixfold coordinated Cd ion in CdO is 2.35 Å, while the bond lengths in  $\text{In}_2\text{O}_3$ ,  $\text{Lu}_2\text{O}_3$ ,  $\text{SnO}_2$ ,  $\text{TiO}_2$ , and  $\text{Al}_2\text{O}_3$  are (in average) 2.20, 2.02, 1.96, and 1.96 Å, respectively. We

TABLE I. Largest component,  $V_{ZZ}$ , of the EFG tensor at the Cd site obtained in the FPLAPW and PAW calculations compared with experimental PAC results at 300 K.  $d(\text{Cd-Onn})$  are the distances from Cd to its Onn.  $Q=0.83(14)$  b (Ref. 43) was used to calculate  $V_{ZZ}$  from the experimental nuclear-quadrupole frequency  $\omega_Q$ . The sign of experimental  $V_{ZZ}$  is unknown.

System		$d(\text{Cd-Onn})$ (Å)	$V_{ZZ}$ ( $10^{21}$ V/m <sup>2</sup> )	$\eta$
SnO:Cd (unrelaxed structure)	FPLAPW, LDA	2.22	+7.7	0.00
	FPLAPW, GGA	2.22	+7.7	0.00
	PAW	2.22	+7.5	0.00
SnO:Cd (relaxed structure)	FPLAPW, LDA	2.27	+6.2	0.00
	FPLAPW, GGA	2.31	+2.4	0.00
	PAW	2.35	+0.4	0.00
SnO:Cd	PAC results <sup>a</sup>		8.2(3)	0.00

<sup>a</sup>Reference 23.

clearly see a correlation among these movements where the presence of the Cd impurity favors the reconstruction of the bond lengths of Cd in its own oxide, CdO.

As we mentioned before, in the PAW calculations, no symmetry constraints are imposed on the atomic relaxations. We see from Table I that the distance Cd-Onn is enlarged from 2.22 to 2.35 Å, which is slightly larger than those predicted by the FPLAPW calculation using the same GGA functional. It is worth mentioning that CP-PAW also predicted a larger Sn-O bond length in pure SnO and SnO<sub>2</sub>.<sup>36</sup>

The relaxation process reduces the magnitude of  $V_{ZZ}$ , as can be seen from the results presented in Table I. In opposition to what has been observed in the case of the unrelaxed structure, the  $V_{ZZ}$  results obtained in the three calculations performed here are very different. There is a clear decrease in magnitude going from LDA to GGA, and the  $V_{ZZ}$  result obtained using the PAW code is close to zero. This apparent discrepancy in the EFG value furnished by the two state-of-the-art theoretical approaches can be easily understood. In the case of the unrelaxed structure where the calculations were performed with the same atomic positions, we have found similar EFGs in all calculations, but, in the case of the relaxed structures, slightly different equilibrium structures were predicted. These results indicate that the different  $V_{ZZ}$  values obtained in this case can be related to different equilibrium structures better than the different descriptions of the electronic structure of the doped system. To support this assertion, we have performed a series of calculations: (a) we took the equilibrium structure predicted by FPLAPW-GGA and, with these positions, we performed a FPLAPW-LDA calculation, obtaining in this case  $V_{ZZ}=+2.3 \times 10^{21}$  V/m<sup>2</sup>, the same result obtained in FPLAPW using the GGA parametrization ( $V_{ZZ}=+2.4 \times 10^{21}$  V/m<sup>2</sup>); (b) a FPLAPW-GGA calculation at the equilibrium positions predicted by FPLAPW-LDA, obtaining  $V_{ZZ}=+6.3 \times 10^{21}$  V/m<sup>2</sup>, which is the same result as in the FPLAPW-LDA calculation ( $V_{ZZ}=+6.2 \times 10^{21}$  V/m<sup>2</sup>); (c) a FPLAPW-LDA calculation using the equilibrium positions predicted by PAW and the  $V_{ZZ}=+0.57 \times 10^{21}$  V/m<sup>2</sup> obtained is in excellent agreement with the PAW predictions for these atomic positions; (d) a PAW calculation at the relaxed position obtained in the FPLAPW-LDA calculations and the  $V_{ZZ}=+6.1 \times 10^{21}$  V/m<sup>2</sup> value is again in excellent agreement with the FPLAPW-LDA result ( $V_{ZZ}=+6.2 \times 10^{21}$  V/m<sup>2</sup>). From these tests, we can conclude that, when we use the same structural positions, FPLAPW-LDA, FPLAPW-GGA, and PAW predict the same EFG tensor and, as a consequence, the same electronic structure of the Cd-doped SnO system. The differences observed in Table I can then be associated with the different equilibrium structures predicted in each calculation. These results are very interesting since small changes in the atomic positions (especially of oxygen atoms closest to Cd) produce large changes in the EFG tensor. It is clear in this case that a precise determination of  $V_{ZZ}$  can be used to obtain a good modeling of the structural relaxations. This is a nice illustration of how the combination of a carefully performed hyperfine technique and a realistic calculation (like the AE ones presented here) of the EFG may be used to obtain structural relaxations with a precision smaller than 0.05 Å.

Before discussing our theoretical results in the light of the measurements, let us briefly critically review the experimen-

tal information. The only available PAC result for Cd-doped SnO was obtained by Rentería *et al.*<sup>23</sup> As we mentioned in Sec. I, these experimental results presented serious problems concerning the analysis of the SnO phase. In effect, different phases coexisted in the sample, and as a consequence, multiple interactions (four) were necessary to reproduce the whole set of experimental results. One interaction (that appeared in these films within a very small window of annealing treatments) was characterized by  $\eta=0.00$ . This is the expected symmetry for Cd located at cationic sites of crystalline SnO, and then this interaction was attributed to Cd in SnO. The quadrupole frequency of this interaction was determined to be  $\omega_Q=25.1$  Mrad/s. It is important to note that this interaction showed an EFG distribution which varied between 4% and 25% and represented only 10% of the probes implanted in the films. Also, the PAC spectra were very dampened along all the experiment. Under these circumstances, it is very difficult to guarantee the  $\eta=0.00$  value reported for that interaction.

If we compare our theoretically relaxed  $V_{ZZ}$  values with the available experimental result [ $V_{ZZ}^{\text{expt}}=8.23 \times 10^{21}$  V/m<sup>2</sup> (Ref. 23)], we see that the FPLAPW and PAW predictions are not in conclusive agreement with the experimental results. As we established in Sec. III, FPLAPW and PAW correctly describe the EFG in pure SnO. Moreover, FPLAPW calculations of the EFG successfully predicted the EFG at Cd impurity sites in TiO<sub>2</sub>,<sup>13,14</sup> SnO<sub>2</sub>,<sup>18</sup> In<sub>2</sub>O<sub>3</sub>,<sup>19</sup> Lu<sub>2</sub>O<sub>3</sub>,<sup>20</sup> and Al<sub>2</sub>O<sub>3</sub>.<sup>21</sup> Since the reported experiments are not conclusive about the hyperfine interaction assigned to substitutional Cd located at cationic sites of crystalline SnO that are free of defects, we suggest that new and accurate experiments are necessary to solve this puzzle.

## V. CHARGE STATE OF THE IMPURITY

In our calculations, a last issue to be considered is the charge state of the impurity. In the calculations presented in previous sections, we assumed that when a neutral Cd substitutes Sn in SnO, it takes the same oxidation state as Sn in this compound. We will name this charge state “neutral charge state” ( $q=0$ ). In this neutral charge state, as we show in Fig. 2(b), the impurity state located at the top of the valence band is occupied and the impurity level at the bottom of the conduction band is empty. However, it is known that the presence of defects (vacancies, interstitial Cd or Sn atoms, metallic impurities with acceptor O donor character, etc.) can modify the impurity charge state. As it was demonstrated in Refs. 13 and 14, the charge state of the impurity can modify the structural relaxations around the impurity and strongly affect the EFG. In order to investigate this point, we have performed two additional calculations using the WIEN97 code in the LDA approximation, removing ( $q=+1$ ) or adding ( $q=-1$ ) one electron to the whole system. The corresponding total DOSs for the two charge states studied here (besides the neutral one) are shown in Fig. 4.

We should mention here that, depending on the charge state, Cd complexes in Si and Ge (investigated by the Korringa-Kohn-Rostoker–Green function approach) have shown a local magnetic moment, leading to a small but siz-

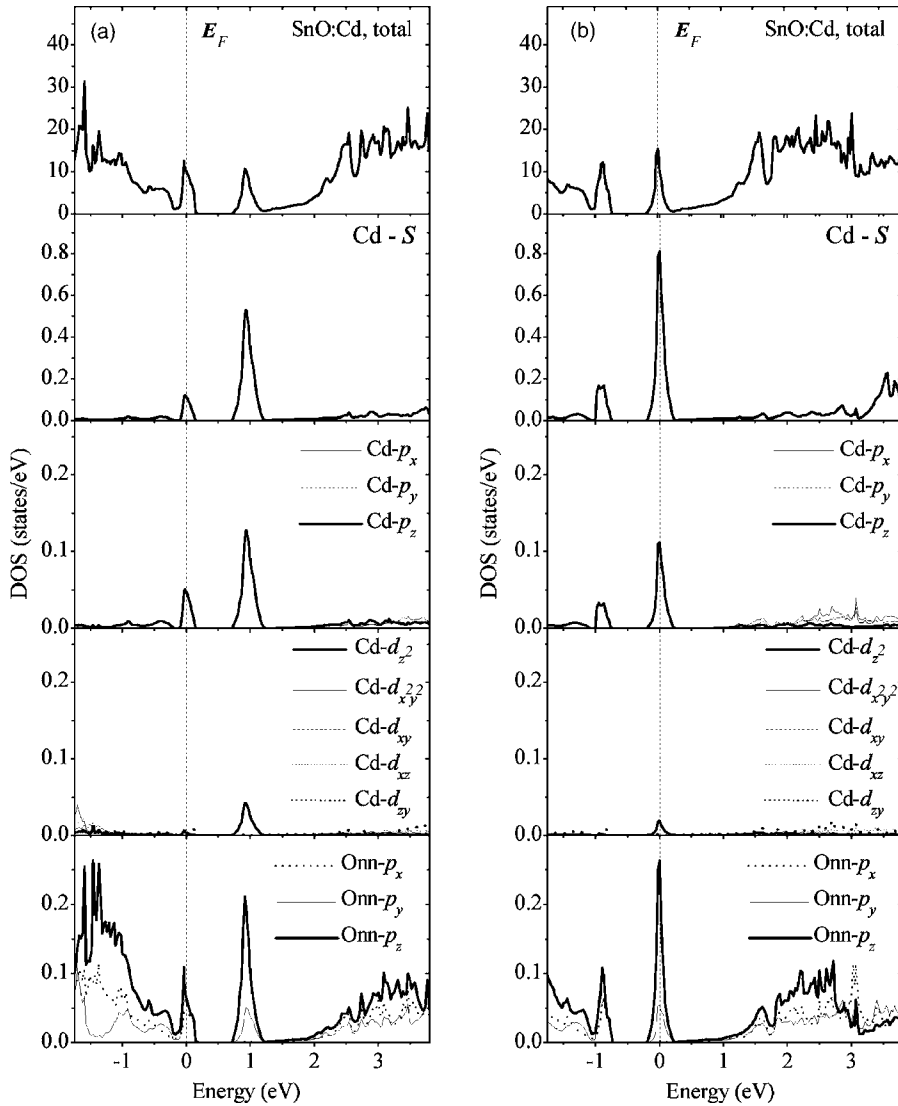


FIG. 4. Total DOS and atom-resolved PDOS at Cd and its Onn atoms in the relaxed 32-atom SC for (a)  $q=+1$  and (b)  $q=-1$ . Energies are referred to the Fermi level ( $E_F$ ).

able hyperfine field at the Cd site.<sup>22</sup> A magnetic signal should then be observed whenever a localized state is occupied by a single electron. We note, however, that, although we have also performed spin-polarized calculations, no magnetic moment was found here. Since we are using the SC approximation, the localized state is broadened, which might have quenched the moment present in the extreme dilute limit, as discussed by Höhler *et al.*<sup>22</sup> Larger SC for Cd-doped SnO could be studied in a forthcoming paper in order to investigate the influence of the dilution into the magnetic behavior. Nevertheless, new PAC measurements could also shed some light into this issue.

As can be seen when comparing the results presented in Figs. 4(a) and 4(b), there is an almost “rigid band” behavior of the DOS, where the removal of one electron has the only effect of making the impurity level at the top of the valence band half occupied. Nevertheless, the structural relaxation is affected by this change, since the equilibrium Cd-Onn bond length is 2.24 Å and, as a consequence, the EFG is also affected. The result for  $V_{ZZ}$  at the final equilibrium structure for  $q=+1$  we obtained is  $+10.4 \times 10^{21}$  V/m<sup>2</sup>, maintaining the same symmetry and orientation of the EFG tensor as in

the neutral state. On the other hand, when we added one electron to the SC, the impurity level at the bottom of the conduction band becomes half occupied, still showing an overall rigid band behavior, but the extra electron produces an enhancement of the electrostatic repulsion, such that the Cd-Onn distance is enlarged to 2.38 Å. The  $V_{ZZ}$  value in this case presents even a change in sign,  $V_{ZZ}=-4.3 \times 10^{21}$  V/m<sup>2</sup>.

As we discussed in previous sections, the EFG strongly depends on the Cd-Onn distances. Since different charge states produce different structural distortions, it is interesting to separate the electronic and structural effects. In order to do that, we have taken the equilibrium structure of Cd-doped SnO obtained using the FPLAPW with LDA (see Table I) and performed calculations adding and removing one electron to the system without relaxing the structure. Interestingly, we found that the EFG is nearly independent of the charge state of the impurity:  $V_{ZZ}=+5.1 \times 10^{21}$  V/m<sup>2</sup> for  $q=+1$ ,  $V_{ZZ}=+6.2 \times 10^{21}$  V/m<sup>2</sup> for  $q=0$ , and  $V_{ZZ}=+7.2 \times 10^{21}$  V/m<sup>2</sup> for  $q=-1$ . These changes induced by the removal (or addition) of one electron are smaller than those observed when the structural relaxations are considered for a

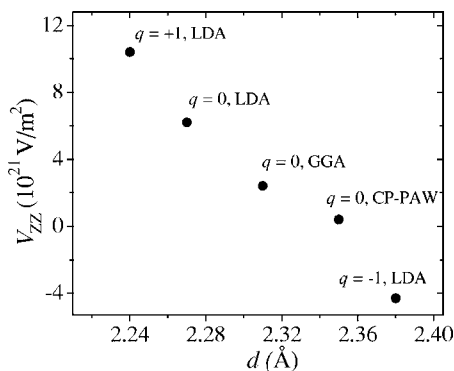


FIG. 5.  $V_{ZZ}$  as a function of the Cd-Onn relaxed bond length ( $d$ ) obtained in the different calculations performed here.

given charge state. These results indicate that the variations in  $V_{ZZ}$  as a function of the charge state are mainly originated in the different structural distortions induced in each case.

The fact that the structural properties play a fundamental role in the EFG can be clearly observed from the results presented in Fig. 5, where all calculated EFGs are plotted as a function of the Cd-Onn distances ( $d$ ). We see that  $V_{ZZ}$  decrease linearly with  $d$ . This behavior can be easily understood due to the dependence of the EFG on  $r^{-3}$  (see, e.g., Ref. 11); if we perform calculations conserving the symmetry of the structure, we will find a linear decrease of  $V_{ZZ}$  with  $d$ . Based on these considerations, we are lead to the conclusion that the different charge states modify the Coulombian interaction between the atoms, but the symmetry distribution of the electronic clouds is mainly unaltered. This can be easily seen in Fig. 4, where the main difference between the DOSs is a shift of the Fermi level. In addition to this first-order effect, there are small changes in the DOSs which should be reflected in the  $V_{ZZ}$  value since we know that differences of the order of 0.01 electrons in the occupation of different orbitals led to quite different EFG results. These small changes are at the origin of the differences in the  $V_{ZZ}$  magnitude for different impurity charge states for a fixed structure observed here.

## VI. CONCLUSIONS

We have studied the EFG tensor at substitutional Cd impurities in black SnO through state-of-the-art all-electron methods which consider atomic relaxations and the electronic structure in a full-potential approach. We have also considered different charge states of the impurity and its effect on the EFG.

In a behavior similar to what has been observed into other binary oxides, Cd introduces impurity levels in the band gap and induces significant structural distortions in the semiconductor host lattice. The enhancement of the Cd-Onn distance, relative to the original Sn-Onn distance seen here, completes the structural scenario for Cd impurities in binary metal oxides, suggesting that Cd always tends to reconstruct the bond length it has in CdO.

The calculations performed with the FPLAPW and the PAW methods have shown to give always the same EFG

tensor for any given (same) atomic positions and functional (GGA or LDA). Nevertheless, the magnitude of the largest component of the EFG tensor has been shown to be extremely sensitive to fine details of the atomic positions. Due to this fact, when we considered the equilibrium positions predicted by the different methodologies, there was not a unique EFG. We note, however, that the difference among the equilibrium positions in these cases is less than 0.05 Å that bears the current precision reached by x-ray measurements. Our results suggest that a suitable combination of very accurate theoretical and experimental EFG determinations could be used as a powerful tool to probe atomic positions in these cases with a very high degree of accuracy.

We have shown that structural relaxations play a fundamental role in the study of the EFG as a function of the impurity charge state. Since the difference in the occupation of orbitals with different symmetries at the Cd site is almost unaffected by the addition or removal of one electron in SnO:Cd, we could clearly separate here the structural and electronic effects on the EFG in a simple picture. The important effect of the extra electron is to change the Coulomb repulsion: when one electron is added to the system, the Coulomb repulsion increases and, as a consequence, the Cd-Onn distance is enlarged, causing (due to the  $r^{-3}$  dependence of the EFG from the charge sources) a corresponding decrease in the magnitude of the EFG; on the other hand, when one electron is removed, the bond length is reduced and the EFG becomes larger than in the case of the neutral cell.

Since the single available experimental result in the literature is not conclusive and several arguments suggest that the assignment of the hyperfine interaction attributed to Cd atoms located at Sn sites may be wrong, the relatively bad agreement with the very accurate theoretical EFG calculations performed here is not unexpected. Our theoretical results strongly suggest that new PAC experiments using ( $^{111}\text{In} \rightarrow ^{111}\text{Cd}$ ) in pure poly- or single-crystalline SnO samples must be done in order to achieve a conclusive characterization of the EFG at Cd in the crystalline phase of SnO. Through the comparison with the present theoretical results, structural distortions with a very high precision and the charge state of the impurity at 300 K could then be inferred.

## ACKNOWLEDGMENTS

This work was developed under the CAPES (Brazil)-SECyT (Argentina) bilateral agreement (Project No. BR/PA04-EIII/020 and 87/05), and used the computational facilities at the LCCA-USP supported by FAPESP and the IMMP and those of the La Plata's group and Clementina II of SECyT. L.A.E. and M.R. are members of CONICET and acknowledge Agencia Nacional de Promoción Científica y Tecnológica (ANPCyT) for the support under Grant No. PICT98 03-03727, Consejo Nacional de Investigaciones Científicas y Técnicas (CONICET) under Grant No. PEI6174 and PIP6032, Fundación/Antorchas, Argentina, and the Third World Academy of Sciences (TWAS), Italy, under Grant No. RGA 97-057. The authors want to thank Peter Blöchl for making available to us the CP-PAW code.

\*Electronic address: errico@fisica.unlp.edu.ar

†Electronic address: renteria@fisica.unlp.edu.ar

‡Electronic address: hmpetрил@macbeth.if.usp.br

- <sup>1</sup>N. E. Christensen, I. Gorczyca, and A. Svane, *J. Phys. Chem. Solids* **67**, 1948 (2006).
- <sup>2</sup>A. Togo, F. Oba, I. Tanaka, and K. Tatsumi, *Phys. Rev. B* **74**, 195128 (2006).
- <sup>3</sup>M. S. Moreno, R. F. Egerton, J. J. Rehr, and P. A. Midgley, *Phys. Rev. B* **71**, 035103 (2005).
- <sup>4</sup>N. E. Christensen, A. Svane, and E. Peltzer y Blancá, *Phys. Rev. B* **72**, 014109 (2005).
- <sup>5</sup>M. Meyer, G. Onida, M. Palummo, and L. Reining, *Phys. Rev. B* **64**, 045119 (2001).
- <sup>6</sup>E. L. Peltzer y Blancá, A. Svane, N. E. Christensen, C. O. Rodríguez, O. M. Cappannini, and M. S. Moreno, *Phys. Rev. B* **48**, 15712 (1993).
- <sup>7</sup>J. Terra and D. Guenzburger, *Phys. Rev. B* **44**, 8584 (1991).
- <sup>8</sup>X. Q. Pan and L. Fu, *J. Electroceram.* **7**, 35 (2001).
- <sup>9</sup>H. Kawazoe, M. Yasukawa, H. Hyodo, M. Kurita, H. Yanagi, and H. Hosono, *Nature (London)* **389**, 939 (1997).
- <sup>10</sup>S. B. Ogale, R. J. Choudhary, J. P. Buban, S. E. Lofland, S. R. Shinde, S. N. Kale, V. N. Kulkarni, J. Higgins, C. Lanci, J. R. Simpson, N. D. Browning, S. Das Sarma, H. D. Drew, R. L. Greene, and T. Venkatesan, *Phys. Rev. Lett.* **91**, 077205 (2003).
- <sup>11</sup>G. Schatz and A. Weidinger, in *Nuclear Condensed Matter Physics: Nuclear Methods and Applications* (Wiley, Chichester, England, 1996); E. N. Kaufmann and R. J. Vianden, *Rev. Mod. Phys.* **51**, 161 (1979).
- <sup>12</sup>A. Lerf and T. Butz, *Angew. Chem., Int. Ed. Engl.* **26**, 110 (1987); T. Klas, J. Voigt, W. Keppner, R. Wesche, and G. Schatz, *Phys. Rev. Lett.* **57**, 1068 (1986); R. Vianden and U. Feuser, *ibid.* **61**, 1981 (1988); N. Achtziger and W. Witthuhn, *Phys. Rev. B* **47**, 6990 (1993); D. Lupascu, M. Uhrmacher, and K. P. Lieb, *J. Phys.: Condens. Matter* **6**, 10445 (1994); S. Lany, P. Blaha, J. Hamann, V. Ostheimer, H. Wolf, and T. Wichert, *Phys. Rev. B* **62**, R2259 (2000); J. Meererschaut, C. L'abbe, M. Rots, and S. D. Bader, *Phys. Rev. Lett.* **87**, 107201 (2001); J. M. Ramallo López, M. Rentería, E. E. Miró, F. G. Requejo, and A. Traverse, *ibid.* **91**, 108304 (2003); M. Forker, S. Müller, P. de la Presa, and A. F. Pasquevich, *Phys. Rev. B* **68**, 014409 (2003).
- <sup>13</sup>L. A. Errico, G. Fabricius, M. Rentería, P. de la Presa, and M. Forker, *Phys. Rev. Lett.* **89**, 055503 (2002).
- <sup>14</sup>L. A. Errico, G. Fabricius, and M. Rentería, *Phys. Rev. B* **67**, 144104 (2003), and references therein.
- <sup>15</sup>L. A. Terrazos, H. M. Petrilli, M. Marszalek, H. Saitovich, P. R. J. Silva, P. Blaha, and K. Schwarz, *Solid State Commun.* **121**, 525 (2002).
- <sup>16</sup>H. Akai, M. Akai, S. Blügel, B. Drittler, H. Ebert, K. Terakura, R. Zeller, and P. H. Dederichs, *Prog. Theor. Phys. Suppl.* **101**, 11 (1990).
- <sup>17</sup>P. Hohenberg and W. Kohn, *Phys. Rev.* **136**, B864 (1964); W. Kohn and L. J. Sham, *Phys. Rev.* **140**, 1133 (1965).
- <sup>18</sup>L. A. Errico, G. Fabricius, and M. Rentería, *Hyperfine Interact.* **136/137**, 749 (2001).
- <sup>19</sup>L. A. Errico, M. Rentería, G. Fabricius, and G. N. Darriba, *Hyperfine Interact.* **158**, 63 (2004).
- <sup>20</sup>L. A. Errico, M. Rentería, A. G. Bibiloni, and G. N. Darriba, *Phys. Status Solidi C* **2**, 3576 (2005).
- <sup>21</sup>M. Rentería, G. N. Darriba, L. A. Errico, E. L. Muñoz, and P. D. Eversheim, *Phys. Status Solidi B* **242**, 1928 (2005).
- <sup>22</sup>H. Höhler, N. Atodiresci, K. Schroeder, R. Zeller, and P. H. Dederichs, *Phys. Rev. B* **71**, 035212 (2005); **70**, 155313 (2004).
- <sup>23</sup>M. Rentería, A. G. Bibiloni, M. S. Moreno, J. Desimoni, R. C. Mercader, A. Bartos, M. Uhrmacher, and K. P. Lieb, *J. Phys.: Condens. Matter* **3**, 3625 (1991).
- <sup>24</sup>H. Wolf, S. Deubler, D. Forkel, H. Foettinger, M. Iwatschenko-Borho, M. Meyer, M. Renn, and W. Witthuhn, *Mater. Sci. Forum* **10-12**, 863 (1986).
- <sup>25</sup>S. H. Wei and H. Krakauer, *Phys. Rev. Lett.* **55**, 1200 (1985).
- <sup>26</sup>P. E. Blöchl, *Phys. Rev. B* **50**, 17953 (1994); P. E. Blöchl, C. J. Först, and J. Schimpl, *Bull. Mater. Sci.* **26**, 33 (2003).
- <sup>27</sup>X. Wang, F. X. Zhang, I. Loa, K. Syassen, M. Hanfland, and Y.-L. Mathins, *Phys. Status Solidi B* **241**, 3168 (2004).
- <sup>28</sup>P. Blaha, K. Schwarz, P. Dufek, and J. Luitz, WIEN97, Vienna University of Technology, 1997. Improved and updated UNIX version of the original copyrighted WIEN code, which was published by P. Blaha, K. Schwarz, P. I. Sorantin, and S. B. Trickey, *Comput. Phys. Commun.* **59**, 399 (1990).
- <sup>29</sup>J. P. Perdew and Y. Wang, *Phys. Rev. B* **45**, 13244 (1992).
- <sup>30</sup>J. P. Perdew, K. Burke, and M. Ernzerhof, *Phys. Rev. Lett.* **77**, 3865 (1996).
- <sup>31</sup>P. Blaha, K. Schwarz, and P. H. Dederichs, *Phys. Rev. B* **37**, 2792 (1988); K. Schwarz, C. Ambrosch-Draxl, and P. Blaha, *ibid.* **42**, 2051 (1990).
- <sup>32</sup>H. M. Petrilli, P. E. Blöchl, P. Blaha, and K. Schwarz, *Phys. Rev. B* **57**, 14690 (1998).
- <sup>33</sup>M. Alves-Santos, L. Y. A. Dávila, H. M. Petrilli, R. B. Capaz, and M. J. Caldas, *J. Comput. Chem.* **27**, 217 (2006).
- <sup>34</sup>R. Car and M. Parrinello, *Phys. Rev. Lett.* **55**, 2471 (1985).
- <sup>35</sup>H. Haas and H. M. Petrilli, *Phys. Rev. B* **61**, 13588 (2000).
- <sup>36</sup>L. A. Errico, M. Rentería, and H. M. Petrilli, *Physica B* **389**, 37 (2007).
- <sup>37</sup>L. A. Errico, *Physica B* **389**, 140 (2007).
- <sup>38</sup>J. Geurts, S. Rau, W. Richter, and F. J. Schmitte, *Thin Solid Films* **121**, 217 (1984).
- <sup>39</sup>K. M. Krishna, M. Sharon, M. I. K. Mishra, and V. R. Marathe, *Electrochim. Acta* **41**, 1999 (1996).
- <sup>40</sup>P. E. Lippens, J. Olivier-Fourcade, and J. C. Jumas, *Hyperfine Interact.* **126**, 137 (2000).
- <sup>41</sup>M. S. Moreno, J. Desimoni, A. G. Bibiloni, M. Rentería, C. P. Massolo, and K. Freitag, *Phys. Rev. B* **43**, 10086 (1991).
- <sup>42</sup>H. Hass, M. Menninger, H. Andreasen, S. Damgaard, H. Grann, F. T. Pedersen, J. W. Petersen, and G. Weyer, *Hyperfine Interact.* **15/16**, 215 (1983).
- <sup>43</sup>P. Herzog, K. Freitag, M. Reuschenbach, and H. Walitzki, *Z. Phys. A* **294**, 13 (1980).